Encapsulation of single plasmonic nanoparticles within ZIF-8 and SERS analysis of the MOF flexibility

Encapsulation of Single Plasmonic Nanoparticles within ZIF-8. SERS Analysis of MOF Flexibility

Guangchao Zheng,[a] Sarah de Marchi,[a] Vanesa López-Puente,[a] Kadir Sentosun,[b] Lakshminarayana Polavarapu,[a] Ignacio Pérez-Juste,[a] Eric H. Hill,[c] Sara Bals,[b] Luis M. Liz-Marzán,[c,d] Isabel Pastoriza-Santos,[a,*] Jorge Pérez-Juste[a,*]

[a] *Departamento de Quıímica Física, Universidade de Vigo, 36310, Spain*

[b] *EMAT-University of Antwerp, Groenenborgerlaan 171, B-2020 Antwerp, Belgium*

[c] *Bionanoplasmonics Laboratory, CIC biomaGUNE, 20009 Donostia-San Sebastián, Spain*

[d] *Ikerbasque, Basque Foundation for Science, 48013 Bilbao, Spain*

Corresponding Authors

pastoriza@uvigo.es (I. Pastoriza-Santos)

juste@uvigo.es (J. Pérez-Juste)

ABSTRACT

Hybrid nanostructures composed of metal nanoparticles and metal-organic frameworks (MOFs) have recently received increasing attention toward various applications due to the combination of optical and catalytic properties of nanometals with the large internal surface area, tunable crystal porosity and unique chemical properties of MOFs. Encapsulation of metal nanoparticles of well defined shapes into porous MOFs in a core-shell type configuration can thus lead to enhanced stability and selectivity in applications such as sensing or catalysis. In this study, we demonstrate the encapsulation of single noble metal nanoparticles with arbitrary shapes within zeolitic imidazolate-based metal organic frameworks (ZIF-8). The synthetic strategy is based on the enhanced interaction between ZIF-8 nanocrystals and metal nanoparticle surfaces covered by quaternary ammonium surfactants. High resolution electron microscopy and electron tomography confirmed a complete core-shell morphology. Such a well-defined morphology allowed us to study the transport of guest molecules through the ZIF-8 porous shell by means of surface enhanced Raman scattering (SERS) by the metal cores. Our results demonstrate that even molecules larger than the ZIF-8 aperture and pore size may be able to diffuse through the framework and reach the metal core.

KEYWORDS: Metal-Organic Frameworks, Plasmonic nanoparticles, nanocomposites, molecular sieves, SERS, Catalysis

Metal organic frameworks (MOFs) are highly relevant materials for applications in catalysis, gas storage/separation, drug delivery, and chemical sensing, among others.[1,2] These materials possess a number of advantages such as rich surface chemistry,[3] high structural versatility[4] and tunable pore size,[5] as compared to more traditional porous materials (mesoporous silica, zeolites or porous carbon). A number of MOF compounds exhibit structural flexibility and dynamic behavior, thereby raising new possibilities in various fields.[6] This is the case of some zeolitic imidazolate frameworks (ZIFs), such as ZIF-8 ($(Zn(MeIM)_2$, MeIM = 2-methylimidazole). Several reports indicate that the aperture of ZIF-8 is rather flexible at room temperature, presumably due to rotation of the MeIM ligand upon pressure increase or introduction of guest molecules.[7] As a consequence, ZIF-8 does not exhibit a sharp molecular sieving "cut-off" at 3.4 Å (nominal crystallographic aperture size for ZIF-8). Interestingly, there is some controversy in the literature, related to the incorporation of guest molecules into MOFs by diffusion. In general, the diffusion of guest molecules is limited to those that are smaller than the MOF aperture size, but it has been occasionally reported that molecules larger that both aperture and pore sizes can be successfully incorporated.[8,9] Recent adsorption and diffusion studies of a series of probe molecules have demonstrated the framework flexibility of ZIF-8, finding a molecular sieving effect in the molecular size range of 4-6 Å.[10]

The integration of inorganic nanoparticles within MOFs offers the opportunity of creating multifunctional materials with novel or enhanced properties.[11-13] Different approaches have thus been proposed for the encapsulation of metal nanoparticles in MOFs,[14,15] including liquid/gas-phase infiltration methods where the MOF is exposed to a metal precursor that diffuses into its nanopores and subsequently gets either reduced or decomposed into the corresponding metal nanoparticles. Such impregnation approaches however lack precise control over nanoparticle shape, size and composition. Alternatively, nanoparticle-MOF composites can be obtained via encapsulation of preformed nanoparticles by MOFs. This process requires incorporation of the particles during the nucleation and growth of MOF crystals. Since the homogeneous nucleation of MOFs competes with their heterogeneous growth on the nanoparticles surface, the

affinity between both systems is critical.[13] Different capping agents, such as 1-mercaptoundecanoic acid (MUA) or polyvinylpyrrolidone (PVP), have been reported to provide the nanoparticles with enhanced affinity and to promote their interaction with MOFs,[16-18] while preserving colloidal stability in the reaction medium. Importantly, the size, shape and composition of the encapsulated nanoparticles are maintained during encapsulation, thereby keeping their intrinsic properties while MOF formation further enhances the colloidal stability of the system. Therefore, nanoparticle-MOF hybrids encompass the unique properties of individual nanoparticles with the molecular sieving behavior of MOFs. For instance, Lu et al.[16] proposed a method to incorporate multiple nanoparticles, though maintaining their individuality, in ZIF-8 nanocrystals formed by assembly of zinc ions and 2-methylimidazolate in methanol. Encapsulation was mediated by surface modification of the nanoparticles with PVP. Few reports deal however with the encapsulation of isolated noble metal nanoparticles within MOF crystals (noble metal@MOF). Hu et al.[19] proposed a surfactant mediated method for the MOF coating of single gold octahedra and He et al. reported the preparation of core-shell Au@MOF-5 by mixing gold and MOF precursors in the reaction solution and controlling their respective growth rates.[20] As yet, general procedures to encapsulate particles with arbitrary shape and composition are not sufficiently developed.

We report a simple and general approach to synthesize metal@ZIF-8 hybrids, in which preformed plasmonic nanoparticles with well-defined compositions and morphologies are individually encapsulated within ZIF-8 crystals, without affecting their crystalline structure. A key issue is the presence of a quaternary ammonium surfactant (C_nTA) at the metal nanoparticle surface, which promotes the interaction with ZIF-8, leading to MOF nucleation and growth on the particles' surface. This approach can be readily extended to C_nTA-stabilized plasmonic nanoparticles with arbitrary shape and composition. We also investigated the effect of CTAB concentration on the thickness of the ZIF-8 shell. Additionally, the plasmonic properties of the encapsulated nanoparticles allowed us to gain better insight into the molecular sieving effect, i.e. the size-selective diffusion of molecules through ZIF-8, by means of surface enhanced Raman scattering (SERS). This effect is likely to provide important information

about the flexibility of the ZIF-8 structure and to help understanding processes occurring in MOFs in relation with catalysis, sensing, drug delivery or chemical separation. *Ab initio* calculations predict a stable configuration once the guest molecules are incorporated inside the ZIF-8 pores.

RESULTS AND DISCUSSION

The individual encapsulation of plasmonic nanoparticles within ZIF-8 crystals involves the synthesis of plasmonic nanoparticles of the desired size, shape and composition, stabilized with quaternary ammonium surfactants (C_nTA), followed by the controlled crystallization of ZIF-8 on the metal surface. On one hand, quaternary ammonium surfactants have been shown to play an important role in promoting the synthesis of ZIF-8 crystals of various sizes and shapes, in water.[21] While the C_nTA concentration (always below the critical micelle concentration, *cmc*) can be used to modulate the MOF crystal size, the hydrophobic hydrocarbon chain gets preferentially adsorbed on the MOF {100} facets, leading to formation of cubic structures.[21] On the other hand, quaternary ammonium surfactants are commonly used as capping agents for the synthesis of metal nanoparticles, C_nTA molecules being known to form a bilayer structure on the nanoparticles surface.[22] Therefore, C_nTA surfactants are likely to promote the interaction between the metal surface and ZIF-8, as previously reported.[19] It should be noted however that careful control of the surfactant concentration in the reaction mixture was required to successfully encapsulate single metal nanoparticles within ZIF-8 crystals. The C_nTA concentration should be maintained below the *cmc,* as otherwise nucleation and growth of ZIF-8 would be strongly hindered, leading to formation of small ZIF-8 crystals (< 10 nm) in solution and non-homogenous coating of the metal nanoparticles (see Figure S1). Figure 1 displays representative TEM images of the encapsulation of individual metal nanoparticles by ZIF-8, in the presence of cethyltrimethylammonium bromide ($C_{16}TAB$, see Methods for details). The same strategy was applied to particles made of different metals (gold and silver) and with different morphologies (nanorods, nanostars and nanospheres), invariably obtaining core-shell colloidal nanocomposites with narrow size distributions. Interestingly, the nanoparticles were found to be individually encapsulated within several cubic ZIF-8 crystals as observed by scanning

electron microscopy SEM (Figure S2) for ZIF-8 coated Au@Ag core-shell (Au@Ag@ZIF-8) nanorods (NRs). The morphology of the coating could be ascribed to multiple ZIF-8 nucleation and/or attachment on the metal surface and further growth of separate nuclei in different directions.

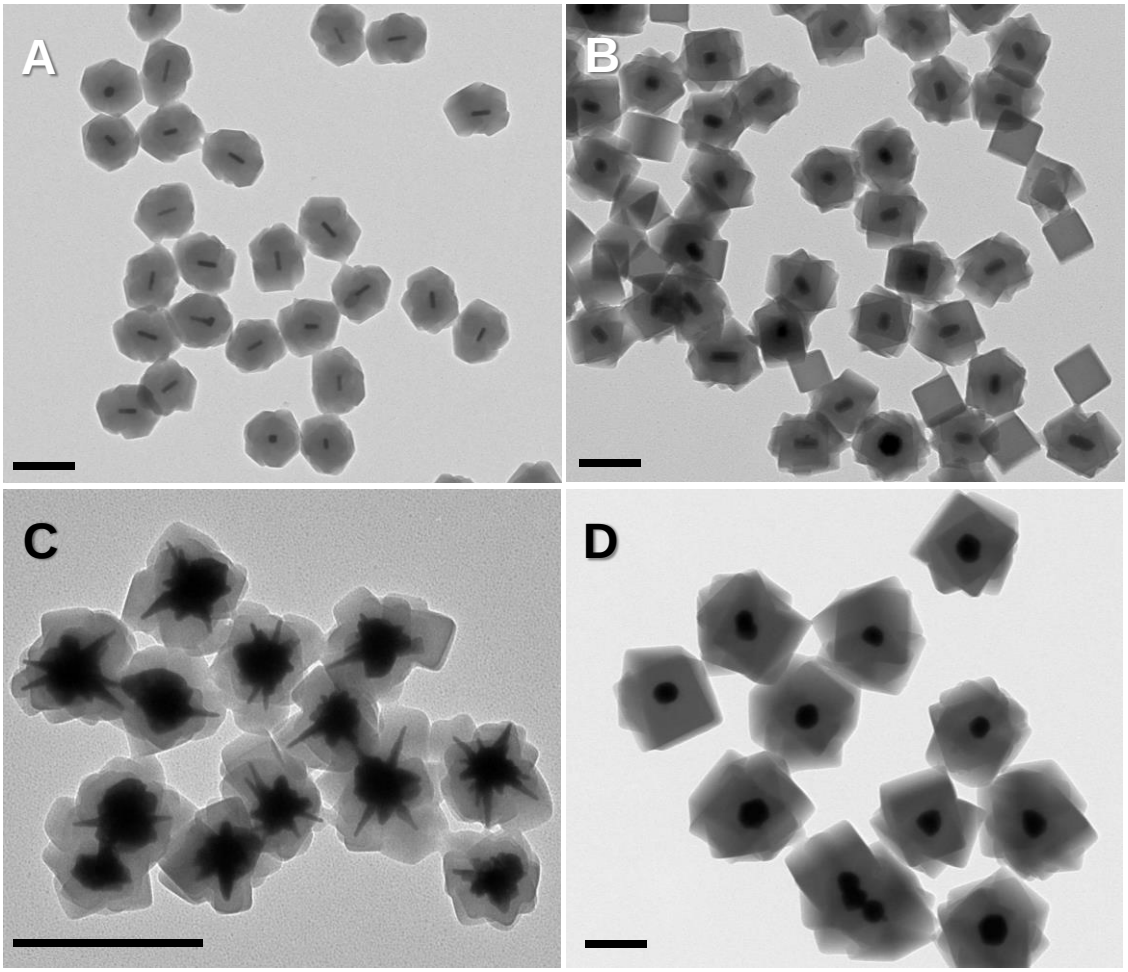

Figure 1. Representative TEM images of different nanoparticles encapsulated in ZIF-8 crystals: (A) gold nanorods, (B) Au@Ag core-shell nanorods, (C) gold nanostars, and (D) gold nanospheres. Scale bars represent 200 nm.

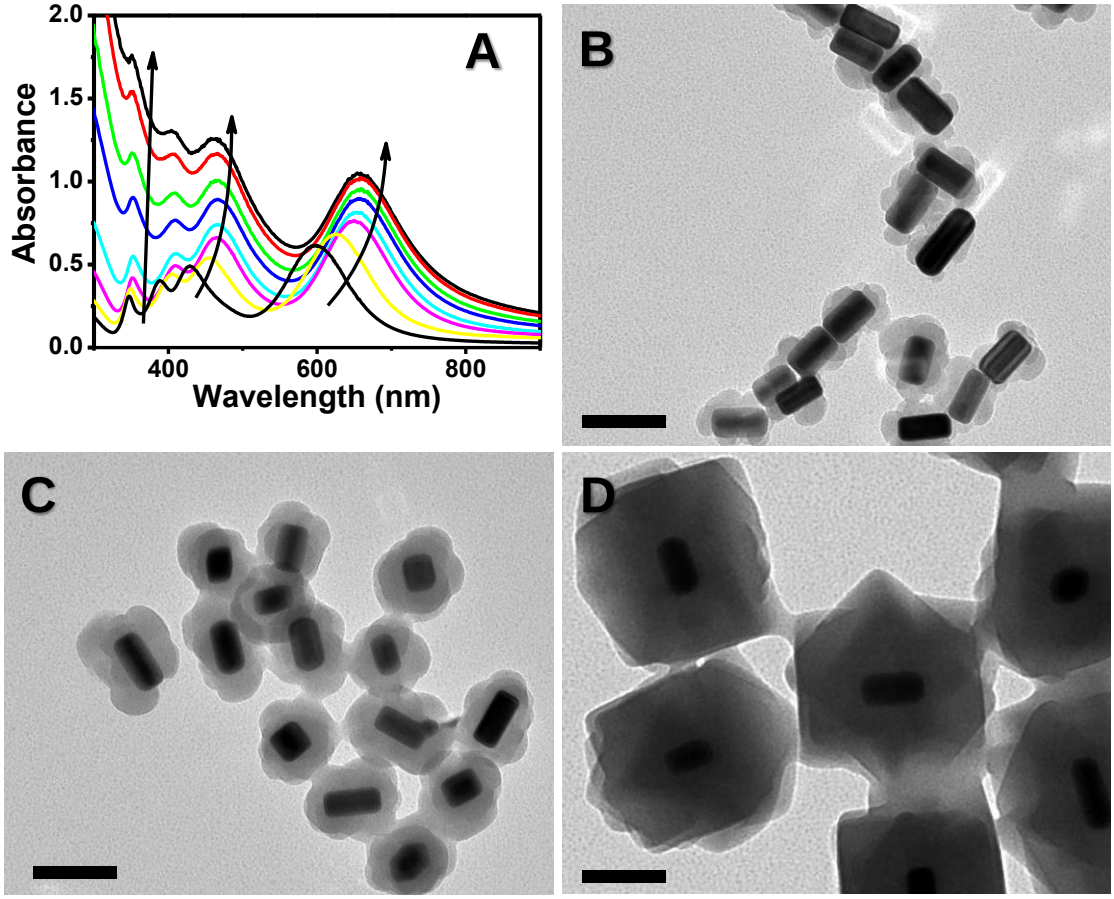

Figure 2. (A) Time evolution of the UV-vis spectra of Au@Ag nanorods during ZIF-8 coating. (C-D) Representative TEM images at different coating times: 5 min (C), 30 min (D) and 3 hours (E). Scale bars represent 100 nm.

With the aim of proposing a growth mechanism, the encapsulation of Au@Ag core-shell NRs with ZIF-8 was monitored by TEM and UV-vis spectroscopy. Figure 2 shows the time evolution of the optical spectra of an aqueous dispersion of Au@Ag NRs during ZIF-8 crystallization, together with representative TEM images of Au@Ag@ZIF-8 intermediates obtained at different reaction times. TEM analysis revealed that after 5 minutes small ZIF-8 nanocrystals were attached to the nanorods' surface (Figure 2B) indicating multiple nucleation/attachment. As the reaction proceeds, all crystals grow simultaneously, leading to the formation of a continuous ZIF-8 shell around the particles (Figure 2C,D). The coating process results in a gradual redshift in the longitudinal surface plasmon resonance of the nanorods, up to 60 nm (from 600 to 660 nm, Figure 2A) as well as an increase in the intensity, especially at lower

wavelengths. While the redshift is expected to originate from the higher refractive index of ZIF-8 (ca. 1.54) as compared to water,[23] the higher absorbance at lower wavelength is due to increased light scattering arising from the larger size of the particles in the dispersion (ZIF-8 crystals and ZIF-8-encapsulated nanoparticles). This scattering contribution was observed to decrease after removing free ZIF-8 crystals by centrifugation. A similar optical behavior was observed for other ZIF-8-coated nanoparticles (see Figure S3 for Au NRs).

The size of ZIF-8 crystals could be modulated by simply varying the concentration of CTAB (always below the *cmc*), which allowed us to tune the thickness of the ZIF-8 shell coating the metal nanoparticles. Figure S4 shows representative TEM mages of Au@Ag core-shell NRs coated with ZIF-8, obtained in the presence of different C_{16}TAB concentrations (0.046 mM, 0.23 mM and 0.46 mM). By varying the C_{16}TAB concentration it was possible to tune the ZIF-8 shell thickness within the range between 16 and 80 nm. Interestingly, no obvious changes in ZIF-8 shell thickness were observed when different concentrations of C_{16}TAC (cetyltrimethylammonium chloride) were used instead of C_{16}TAB (Figure S5), indicating that the selection of counterions may also be critical in the nucleation and growth of ZIF-8.

The characterization of ZIF-8 encapsulated nanoparticles was complemented by powder X-ray diffraction (XRD) analysis. Figure S6 shows the experimental XRD patterns of dried Au NR@ZIF-8 nanoparticles, together with simulated patterns for Au and ZIF-8 crystals. Both patterns, originating from the ordered porous structure of the ZIF-8 shells (2θ = 5-35°)[24] and from the Au cores (2θ = 35-50°), were identified for the core-shell nanostructure. This confirmed the sodalite zeolite-type crystal structure of the ZIF-8 shells and the well-defined peaks in the XRD pattern indicate high crystallinity. Selected area electron diffraction (SAED) was additionally performed on stand-alone ZIF-8 cubes. Since the ZIF-8 morphology changes quickly during electron beam irradiation, the electron dose was kept to a strict minimum. SAED reveals that ZIF-8 nanoparticles are single crystalline with a cubic structure. The SAED pattern in Figure S7, recorded along the [100] zone axis, is in agreement with the previous demonstrated XRD results. The chemical distribution of the elements in the

composite particles was visualized by EDX mapping. Figure 3 shows that Au and Ag are located only at the core whereas Zn is homogeneously distributed in the shell part corresponding to ZIF-8 (Figure 3C-H). The EDX analysis furthermore demonstrates a perfect separation between the Au rod, the Ag shell and the ZIF-8 matrix, i.e. no intermixing of the elements was detected at the boundaries.

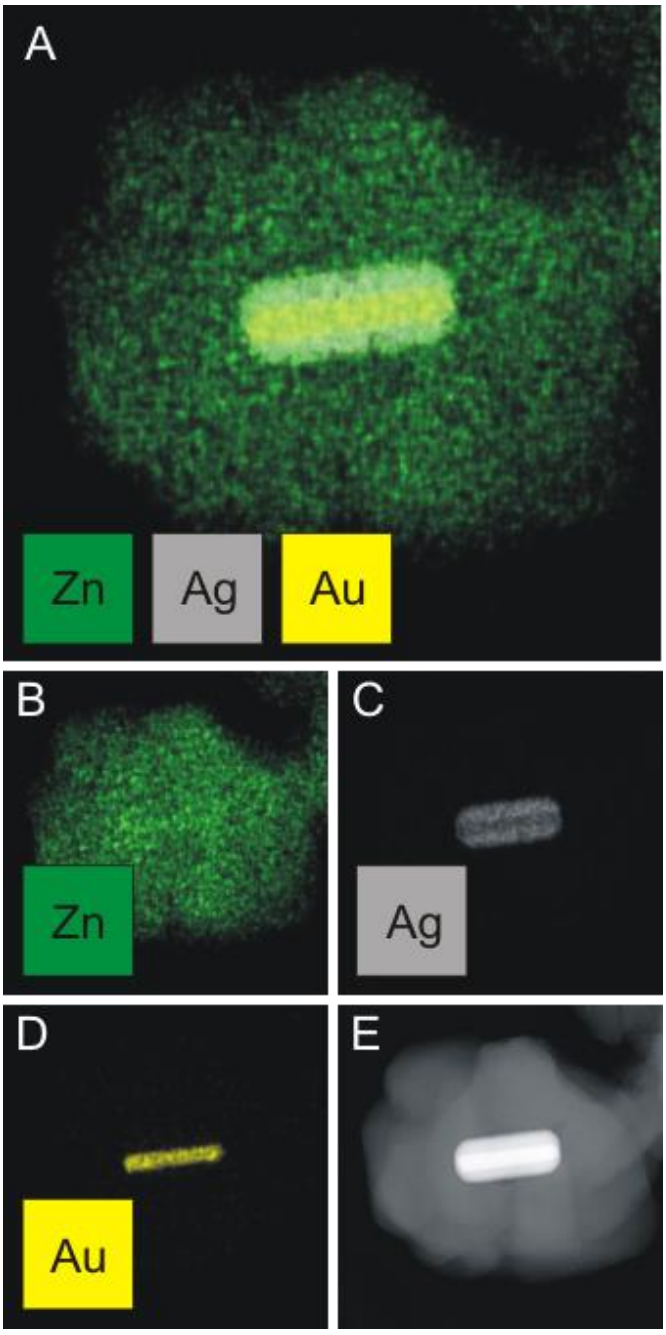

Figure 3. EDX elemental mapping of an Au@Ag@ZIF-8 nanoparticle **(A-D)** and the corresponding HAADF-STEM image **(E)**.

The 3D morphology of the individual nanoparticles was characterized by electron tomography. Multiple detectors (HAADF and ADF) were utilized simultaneously during the acquisition of the tilt series of projection images. In this manner, heavy and light elements in the same sample are both visualized. Furthermore, this technique can be considered as dose efficient, which is of great importance to image these electron beam sensitive materials in 3D.[25] Visualizations along different directions of the 3D reconstruction obtained in this manner are presented in Figure 4 and a video is available as Supporting Information (SV1). The MOF shell is highlighted in green, whereas Ag and Au in the NR are labeled with gray and yellow colors, respectively. In total 5 particles were investigated and it can be concluded that all Au@Ag NRs are entirely surrounded by a MOF shell. Furthermore, the 3D reconstructions reveal that the shell is indeed formed by several ZIF-8 cubes, oriented along different directions. The dimensions of the cubes vary around 110 nm-130 nm. A ZIF-8 coated Au nanorod was also investigated by electron tomography (see Supporting Information video SV2) and EDX (see Figure S8) with similar results, i.e. complete encapsulation of Au nanorod by ZIF-8 and perfect separation of individual elements.

Finally, BET measurements on ZIF-8 and Au@Ag@ZIF-8 particles yielded rather similar values of surface area (1548 $m^2 g^{-1}$ and 1590 $m^2 g^{-1}$ respectively) and pore volume (0.561 $cm^3 g^{-1}$ and 0.585 $cm^3 g^{-1}$, respectively, see Figure S9), which again indicates that the MOF structure is not altered when grown on preformed nanoparticles.

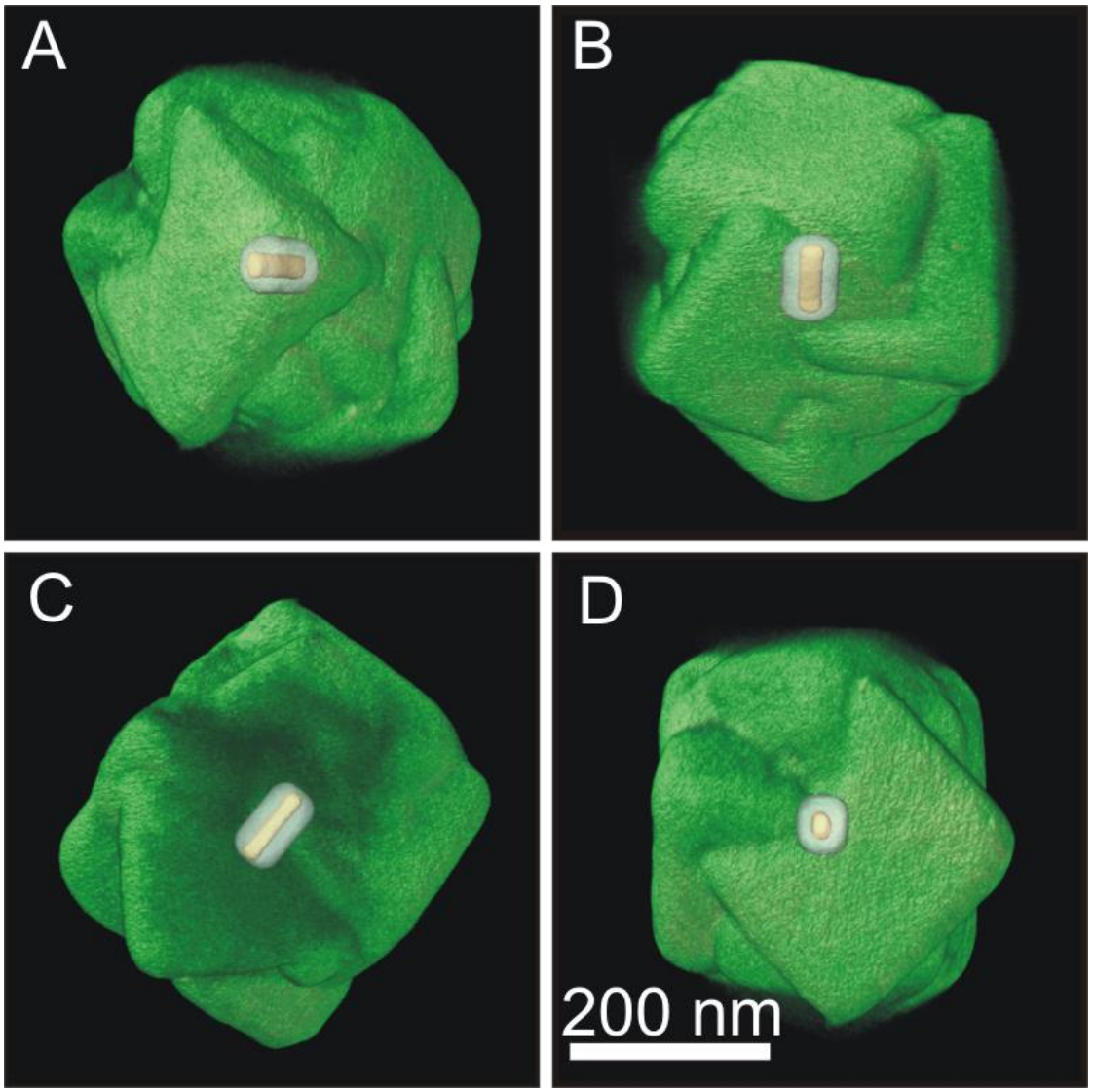

Figure 4. 3D volume representation of a reconstructed ZIF-8 coated Au@Ag core-shell nanoparticle demonstrating the core-shell configuration. See Supporting Information video SV1 for the full reconstruction.

In order to propose a plausible mechanism for the nucleation and growth of ZIF-8 on the metal nanoparticles surface we need to take into account that; on one hand, Pan et al. have shown by molecular dynamics simulations that quaternary ammonium surfactant monomers adsorb preferentially on ZIF-8 facets, following the sequence $\{100\} > \{100\} > \{110\}$. As a result, the growth rate of {100} faces is slower than that of {110} and {111} faces, resulting in ZIF-8 crystals with cubic morphology.[21] On the other hand, Li et al. have shown that ZIF-8 crystals can selectively nucleate and grow on alkanethiol self-assembled monolayers

patterned surfaces.[26] Bearing this in mind and considering that the concentration of CTA monomers in the reaction mixture is below its *cmc* in water (0.9 mM), such a low surfactant concentration should lead to particles stabilized by a monolayer or a sub-monolayer adsorbed on its surface.[27] Under such experimental conditions we postulate that ZIF-8 crystals can selectively nucleate and grow at the surface of the metal nanoparticle due to a favorable interaction between the metal surface and ZIF-8 nanocrystals, mediated by the surfactant. Moreover, the presence of ZIF-8 crystals without a metal core could be due to the nucleation of ZIF-8 induced by surfactant monomers presented in solution.

We finally studied molecular adsorption and diffusion of molecular species into ZIF-8 shells, which is of crucial importance regarding their selectivity and storage capabilities. The ability of guest molecules to diffuse into a mesoporous metal organic framework does not only depend on the sizes of the guest, aperture and pores in the MOF (size selective properties), but also on the flexibility of the framework. Although it has been reported that ZIF-8 presents a flexible framework with a non-sharp molecular sieving “cut-off”, additional evidence is still required. The combination of plasmonic nanoparticles and ZIF-8 crystals allowed us to employ SERS spectroscopy to obtain information on ZIF-8 flexibility through the ability of guest molecules with different sizes to diffuse through the shell and reach the metal surface. Three guest molecules were selected, namely 4-nitrobenzenthiol (NBT), 1-napthalenethiol (1-NAT) and malachite green isothiocyanate (MGI) (molecular structures and sizes are shown in Figure S10). These thiolated aromatic molecules are commonly used Raman probes that can chemically bind to metal surfaces and be easily detected by SERS. Additionally, they feature increasing kinetic diameters of 5.95 Å, 7.20 Å and 13.45 Å for NBT, 1-NAT and MGI, respectively (Figure S10), which allows us to analyze their diffusion properties. Although all the selected guest molecules present kinetic diameters smaller than the ZIF-8 pore size (11.6 Å) they are still larger than the aperture size, 3.4 Å.[28] By means of a semiempirical *ab initio* calculation method (PM7 included in MOPAC2012), we studied the possibility of forming stable inclusion complexes between the target molecules (NBT, 1-NAT and MGI) and the MOF (see Methods for details). The

geometry of the inclusion complexes was first optimized by positioning the molecule in the center of the MOF cage and varying their relative orientation. The interaction energies (E_{int}) were then computed for complexes formed by inclusion of one target molecule inside a ZIF-8 unit cage comprising 708 atoms, using three of the most significant structures for each of the complexes (Figure S11). Such interaction energies were obtained by calculating the energy difference $E_{int} = E_{complex} - E_{ZIF-8} - E_{molecule}$, where $E_{complex}$, E_{ZIF-8} and $E_{molecule}$ are the energy of the complex, ZIF-8 and the molecule, respectively. Therefore, E_{int} with a negative value implied the formation of a stable complex. From the results shown in Table S1, we learn that stable complexes can indeed form between ZIF-8 and NBT, 1-NAT or MGI.

To evaluate the diffusion of the different probe molecules through the ZIF-8 shell, the SERS spectra of NBT, 1-NAT and MGI were measured using a 785 nm excitation laser and using Au@Ag and Au@Ag@ZIF-8 nanoparticles as enhancers (Figure 5A). The spectra obtained with uncoated Au@Ag nanoparticles showed the typical vibrational peaks of each probe molecule (see vibrational assignment in Table S2). The detection of the characteristic SERS spectra for NBT and 1-NAT in the presence of MOF-coated nanoparticles confirmed diffusion through the ZIF-8 shell, all the way to the surface of Au@Ag particles. It should be noted that NBT and 1-NAT could be detected by SERS even though their kinetic diameters are larger than the aperture size. In the case of MGI, which is significantly larger (Figure S10), no SERS peaks were registered, meaning that diffusion was hindered by the shell.

It should be noted that, although the NBT SERS spectrum recorded with Au@Ag@ZIF-8 nanoparticles displayed the same vibrational pattern as that obtained with uncoated Au@Ag nanoparticles, in the case of 1-NAT clear differences were observed in the relative intensity of the signals at 390 cm^{-1} (C-S stretching) and 417 cm^{-1} (ring bending), which are highlighted by a yellow shadowed region in Figure 5A. Interestingly, SERS spectra calculated by DFT for the optimized geometry of a 1-NAT molecule adsorbed on a metallic surface constituted by 24 Ag atoms (Figure S12) showed a good agreement with that experimentally obtained on uncoated Au@Ag nanoparticles. The most stable conformation corresponded to the 1-NAT ring plane oriented in a tilt angle of ca.

30º with respect to the Ag surface. SERS spectra calculated for other restrained orientations of 1-NAT with respect to the metallic surface while keeping constant the S-Ag distance, showed a clear dependence of the relative intensity of the signals at 390 and 417 cm^{-1} with 1-NAT orientation (Figure S11). The theoretical calculations thus indicate that the experimental SERS spectra recorded for 1-NAT in Au@Ag@ZIF-8 nanoparticles may result from a mixture of conformations on the metallic surface, induced by the presence of ZIF-8.

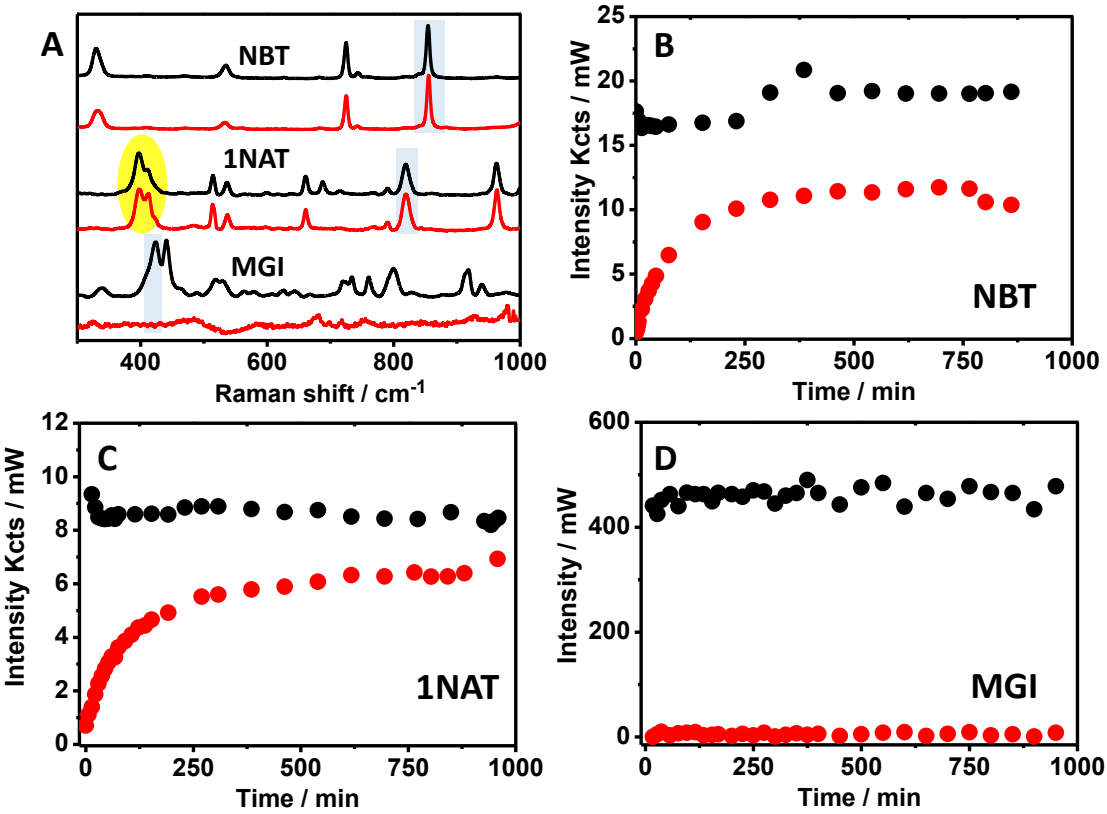

Figure 5. (A) SERS spectra of NBT, 1-NAT and MGI recorded using uncoated (black spectra) and ZIF-8 coated (red spectra) Au@Ag core-shell nanorods. The regions shadowed in blue indicate the bands followed during diffusion studies. The region shadowed in yellow A highlights changes in the SERS spectrum of 1-NAT (see text for details). (B-D) SERS-based kinetic trace of the diffusion of each molecular probe for uncoated (black dots) and ZIF-8 coated (red dots) Au@Ag core-shell nanorods: (B) NBT 854 cm^{-1}, (C) 1-NAT 819 cm^{-1} and (D) MGI 425 cm^{-1}. The data represent averages of three independent measurements for each point.

The diffusion of NBT, 1-NAT and MGI was further analyzed by recording SERS spectra over time. Figure 5B-D shows the time evolution of the Raman scattering modes of NBT, 1-NAT and MGI at 854 cm^{-1}, 819 cm^{-1} and 425 cm^{-1}, respectively (see vibrational assignment in Table S2). The SERS kinetic traces revealed very fast diffusion of the three molecules toward the uncoated nanoparticles surface, whereas the presence of the ZIF-8 shell led to a significantly decreased diffusion rate for NBT and 1-NAT and inhibited the diffusion for the much larger molecule MGI. We therefore conclude that MOF permeability as well as the size of the guest molecules affect the diffusion rate. Interestingly, the molecular diffusion at early times could be fitted to a transient diffusion model with intracrystalline diffusion control (Figure S13), which predicts a quasi-linear kinetic uptake curve, approximated by $[Molecule] \approx Kt^{1/2}$, where K is a constant.[29-31]

The aperture and pore size values reported for ZIF-8 (3.4 Å and 11.6 Å, respectively) were determined on the basis of a crystal structure refinement with the superposition of the van der Waals radii for the atoms. However, it is now accepted for ZIF-8 that the structure is not fixed in a given orientation. Therefore, the aperture size does not necessarily restrict access to molecules of smaller diameter since larger molecules such as NBT or 1-NAT (with kinetic diameters of 5.95 Å and 7.20 Å, respectively) were found to be absorbed by these materials. Different mechanisms have been proposed to explain such diffusion. On one had the dissociative linker substitution of the coordinately saturated metal center might lead to a short-lived ligand vacancy that would expand the pore aperture size allowing the diffusion of the guest (NBT or 1-NAT) into the framework.[8] Indeed, it has been reported that guests with molecular diameters 3-4 times the aperture size were encapsulated into ZIF-8 crystals.[8] On the other hand, lattice dynamics, such as collective vibrations or MOF flexibility, occurring in the ZIF-8 framework could give rise to phenomena such as geometrical distortion, shear deformation or gate opening. While gate opening vibrations could lead to variation in the four membered ring and pore aperture, a soft mode could lead to elongation of the six membered ring.[32,33] Therefore, gating and kinetic trapping processes are unique to flexible MOFs allowing the diffusion of relatively large molecules through the ZIF-8 shell.

CONCLUSION

In summary, we described a general strategy for the encapsulation of individual metal nanoparticles with the MOF ZIF-8. The method can be readily applied to metal particles with arbitrary morphologies, as long as they are capped with a quaternary ammonium surfactant. The hydrophobic hydrocarbon chains of CTA^+ molecules adsorbed on metal surfaces can readily complex with MOF crystals, thereby inducing ZIF-8 nucleation and/or adsorption and further growth on the metal surface. Our results demonstrate that the thickness of the ZIF-8 shell can be tuned through either reaction time or CTAB concentration. Most interestingly, the presence of plasmonic nanoparticles as cores and their SERS enhancing properties allowed us to study the transport of different guest molecules inside the ZIF-8 shell. Analysis of the results showed that molecules such as NBT or 1-NAT followed a transient diffusion model with intracrystalline diffusion control. We additionally demonstrated the ability of ZIF-8 to incorporate molecules moderately larger than the nominal aperture and pore size. We expect that this procedure can be readily extended to other types of MOFs and to be of high relevance in the fields of catalysis and sensing.

METHODS

Chemicals. Hexadecyltrimethylammonium bromide (CTAB, 98%), hexadecyltrimethylammonium chloride solution (CTAC, 25%wt), sodium borohydride (99%), gold (III) chloride trihydrate (99.9%), silver nitrate ($AgNO_3$), L-(+)-ascorbic acid, 2-methylimidazole (2-MIM, 99%), zinc nitrate hexahydrate ($Zn(NO_3)_2{\cdot}6H_2O$, 99%), 1-naphthalenethiol (1-NAT, 99%), and 4-nitrothiophenol (NBT, technical grade 80%) were purchased from Sigma Aldrich. Malachite green isothiocyanate (MGI) was purchased from Life Technologies. Milli-Q water (18.2 MΩ·cm) was used in all the experiments.

Characterization. Optical characterization was performed using an Agilent 8453 UV-Visible spectrophotometer. Conventional TEM images were acquired with a JEOL JEM 1010 microscope operated at 100 kV. Acquisition of the tilt series for electron tomography was performed using a Fischione 2020 single tilt holder and a FEI Tecnai Osiris electron microscope, operating at an

accelerating voltage of 120 kV. The projection images were collected over an angular range between -74° and +73°, with a 3° tilt increment. The tilt series were aligned using the FEI INSPECT 3D software and reconstructed via the simultaneously iterative reconstruction technique implemented in the ASTRA tomography toolbox[38]. During the acquisition of the projection images, ADF and HAADF detectors were simultaneously utilized to retrieve information from both low and high atomic number elements. More information about the complete acquisition and the reconstruction procedure can be found in ref 25. EDX analysis was performed using a FEI Tecnai Osiris electron microscope equipped with Super-X EDX detector, operating at an accelerating voltage of 120 kV.

The molecular sizes of NBT, 1-NAT and MGI were obtained from density functional theory (DFT) geometrical optimizations performed using the B3LYP functional and the 6-311++G** basis set. All the structures were confirmed as energy minima by analysis of their vibrational frequencies.

Synthesis of Au nanorods. Gold nanorods were prepared by a previously reported seed-mediated growth method.[34] In a typical synthesis, a seed solution was first prepared by adding 0.6 mL of freshly prepared ice-cold $NaBH_4$ (0.01 M) solution to an aqueous mixture of 10 mL of CTAB (0.1 M) and 250 µL of $HAuCl_4$ (0.01 M) under vigorous stirring. With addition of $NaBH_4$, the solution color changed from pale yellow to brown, and the resulting seed solution was kept at room temperature for 2 h. For the preparation of Au NRs, a growth solution was prepared by adding to 50 mL of an aqueous CTAB solution (0.1 M) 2 mL of $HAuCl_4$ (0.01 M), 0.1 mL of $AgNO_3$ (0.01 M), 0.32 mL of AA (0.1 M), and 0.8 mL of HCl (1.0 M), sequentially. Then 96 µL of the seed solution was added to the growth solution, which was kept undisturbed at 27 °C for 6 h to complete the growth. Finally, the as prepared gold nanorods were centrifuged twice in water (5000 rpm for 20 min) and redispersed in water (40 mL, final CTAB concentration 0.9 mM).

Synthesis of Au@Ag core-shell Nanorods. Au@Ag core-shell nanorods were synthesized following a previously reported method with slight modifications.[35] Previously synthetized gold nanorods were coated with silver in an aqueous CTAC solution. Briefly, 10 mL of the as prepared Au NRs solution was

centrifuged at 8000 rpm for 20 min and the precipitate redispersed in 10 mL of CTAC (80 mM). This procedure was repeated twice. Subsequently, 10 mL of the obtained dispersion was diluted to 40 mL of CTAC (80 mM) followed by addition of 3.5 mL of L-(+) ascorbic acid solution (0.1 M) and 3.5 mL of $AgNO_3$ (0.01 M). The resulting solution was placed in an oven at 60 °C for 3 h. The solution was cooled down to room temperature and centrifuged twice in water (7000 rpm for 20 min) and finally redispersed in 10 mL of Milli-Q water (final CTAC concentration 0.5 mM).

Synthesis of Au nanostars. The surfactant-free method was used to prepare Au nanostars.[36] A solution of citrate stabilized gold seeds (ca. 15 nm, [Au] = 0.5 mM, 0.3 mL) prepared by the Turkevich method[37] was added to a solution (30 mL) containing $HAuCl_4$ (0.25 mM) and HCl (1 mM, 30 μL), followed by simultaneous addition of $AgNO_3$ (2 mM, 0.3 mL) and ascorbic acid (100 mM, 0.15 mL) under vigorous stirring. To increase the stability of the obtained nanostars, after five minutes a suitable amount of CTAC (32 mM final concentration) was added to the solution. Upon synthesis, the solution was centrifuged (4500 rpm, 30 min) twice to remove excess reactants, and redispersed in water (final CTAC concentration 0.5 mM and [Au] 2.6 mM).

Synthesis of Au NRs@ZIF-8. The ZIF-8 coating of individual metal nanoparticles was based on a previously reported protocol with slight modifications.[19] Typically, 1 mL of an aqueous solution of $Zn(NO_3)_2 \cdot 6H_2O$ (24 mM) and 1 mL of washed Au nanorods were added sequentially to 1 mL of an aqueous solution of 2-methylimidazole (1.32 M). The solution was gently stirred for 5 min and left undisturbed at room temperature for 3 h. The resulting core-shell Au NRs@ZIF-8 particles were centrifuged at 5000 rpm for 10 min, washed with methanol and finally redispersed in methanol (5 mL).

Synthesis of Au@Ag@ZIF-8. The above described protocol was used for the synthesis of Au@Ag@ZIF-8, except that, in order to control the thickness of ZIF-8 shell, a small amount of CTAB (below the *cmc*) was added to the solution of 2-methylimidazole prior to the addition of $Zn(NO_3)_2 \cdot 6H_2O$ and the nanoparticle dispersion. Typically, 0.144 mL of an aqueous solution of CTAB (1 mM, 5 mM and 10 mM) was added to 1 mL of 2-methylimidazole (1.32 M) and

stirred for 5 minutes. Then, 1 mL of $Zn(NO_3)_2 \cdot 6H_2O$ (24 mM) and 1 mL of washed Au@Ag nanorods were added sequentially to the mixture, stirred for 5 min and left undisturbed at room temperature for 3 h. The core-shell Au@Ag@ZIF-8 particles were centrifuged at 5000 rpm for 5 min, washed with 10 mL of methanol and finally redispersed in 5 mL of methanol. The synthesis could be scaled up to 6-fold using this same protocol.

Synthesis of Au Nanostars@ZIF-8. Typically, 0.144 mL of an aqueous solution of CTAB 1 mM was added to 1 mL of an aqueous solution of 2-methylimidazole (1.32 M) and stirred for 5 min. Subsequently, 1 mL $Zn(NO_3)_2 \cdot 6H_2O$ (24 mM) and 1 mL Au nanostars were added, stirred for 5 min and left undisturbed for 3 h. Finally, Au nanostars@ZIF-8 particles were centrifuged at 5000 rpm for 5 min, washed with 10 mL of methanol and redispersed in 5 mL of methanol.

SERS measurements. SERS experiments were conducted in a micro-Renishaw InVia Reflex system. The spectrograph uses high resolution grating (1200 grooves cm^{-1}) with additional band-pass filter optic, a confocal microscope and a 2D-CCD camera. A laser excitation wavelength of 785 nm (diode) was used for all the measurements. For diffusion experiments, 10 µL aliquot of NBT, 1-NAT or MGI (1 mM) was added to 1 mL of metal@ZIF-8 particles and SERS spectra were collected by using a Renishaw macrosampler accessory. Typically, 10 µL aliquot of 1 mM NBT, 1-NAT or MGI was added to 1 mL of metal@ZIF-8 particles.

ASSOCIATED CONTENT

Supporting Information. This material is available free of charge via the Internet at http://pubs.acs.org

AUTHOR INFORMATION

Corresponding Authors

pastoriza@uvigo.es (I. Pastoriza-Santos)

juste@uvigo.es (J. Pérez-Juste)

ACKNOWLEDGMENT

This work was supported by the Spanish Ministerio de Economía y Competitividad (MAT2013-45168-R) and the Xunta de Galicia/FEDER (Grant No. GPC2013-006; INBIOMED-FEDER “Unha maneira de facer Europa”). LML-M acknowledges funding from the European Union's Seventh Framework Programme (FP7/2007-2013 under grant agreement n° 312184, SACS). S.B. acknowledges financial support from European Research Council (ERC) (ERC Starting Grant No. 335078-COLOURATOM).

REFERENCES

(1) Furukawa, H.; Cordova, K. E.; O'Keeffe, M.; Yaghi, O. M. The Chemistry and Applications of Metal-Organic Frameworks. *Science* **2013**, *341*, 974-+.

(2) Kreno, L. E.; Leong, K.; Farha, O. K.; Allendorf, M.; Van Duyne, R. P.; Hupp, J. T. Metal-Organic Framework Materials as Chemical Sensors. *Chem. Rev.* **2012**, *112*, 1105-1125.

(3) Zacher, D.; Schmid, R.; Woll, C.; Fischer, R. A. Surface Chemistry of Metal-Organic Frameworks at the Liquid-Solid Interface. *Angew. Chem. Int. Ed.* **2011**, *50*, 176-199.

(4) Haldar, R.; Maji, T. K. Metal-Organic Frameworks (Mofs) Based on Mixed Linker Systems: Structural Diversities Towards Functional Materials. *CrystEngcomm* **2013**, *15*, 9276-9295.

(5) Deng, H. X.; Grunder, S.; Cordova, K. E.; Valente, C.; Furukawa, H.; Hmadeh, M.; Gandara, F.; Whalley, A. C.; Liu, Z.; Asahina, S.; Kazumori, H.; O'Keeffe, M.; Terasaki, O.; Stoddart, J. F.; Yaghi, O. M. Large-Pore Apertures in a Series of Metal-Organic Frameworks. *Science* **2012**, *336*, 1018-1023.

(6) Chang, Z.; Yang, D. H.; Xu, J.; Hu, T. L.; Bu, X. H. Flexible Metal-Organic Frameworks: Recent Advances and Potential Applications. *Adv. Mater.* **2015**, *27*, 5432-5441.

(7) Fairen-Jimenez, D.; Moggach, S. A.; Wharmby, M. T.; Wright, P. A.; Parsons, S.; Duren, T. Opening the Gate: Framework Flexibility in Zif-8

Explored by Experiments and Simulations. *J. Am. Chem. Soc.* **2011**, *133*, 8900-8902.

(8) Morabito, J. V.; Chou, L. Y.; Li, Z. H.; Manna, C. M.; Petroff, C. A.; Kyada, R. J.; Palomba, J. M.; Byers, J. A.; Tsung, C. K. Molecular Encapsulation Beyond the Aperture Size Limit through Dissociative Linker Exchange in Metal-Organic Framework Crystals. *J. Am. Chem. Soc.* **2014**, *136*, 12540-12543.

(9) Kreno, L. E.; Greeneltch, N. G.; Farha, O. K.; Hupp, J. T.; Van Duyne, R. P. Sers of Molecules That Do Not Adsorb on Ag Surfaces: A Metal-Organic Framework-Based Functionalization Strategy. *Analyst* **2014**, *139*, 4073-4080.

(10) Zhang, K.; Lively, R. P.; Zhang, C.; Chance, R. R.; Koros, W. J.; Sholl, D. S.; Nair, S. Exploring the Framework Hydrophobicity and Flexibility of Zif-8: From Biofuel Recovery to Hydrocarbon Separations. *J. Phys. Chem. Lett.* **2013**, *4*, 3618-3622.

(11) Liu, Y. L.; Tang, Z. Y. Multifunctional Nanoparticle@Mof Core-Shell Nanostructures. *Adv. Mater.* **2013**, *25*, 5819-5825.

(12) Kuo, C. H.; Tang, Y.; Chou, L. Y.; Sneed, B. T.; Brodsky, C. N.; Zhao, Z. P.; Tsung, C. K. Yolk-Shell Nanocrystal@Zif-8 Nanostructures for Gas-Phase Heterogeneous Catalysis with Selectivity Control. *J. Am. Chem. Soc.* **2012**, *134*, 14345-14348.

(13) Sugikawa, K.; Nagata, S.; Furukawa, Y.; Kokado, K.; Sada, K. Stable and Functional Gold Nanorod Composites with a Metal-Organic Framework Crystalline Shell. *Chem. Mater.* **2013**, *25*, 2565-2570.

(14) Hu, P.; Morabito, J. V.; Tsung, C. K. Core-Shell Catalysts of Metal Nanoparticle Core and Metal-Organic Framework Shell. *ACS Catal.* **2014**, *4*, 4409-4419.

(15) Moon, H. R.; Lim, D. W.; Suh, M. P. Fabrication of Metal Nanoparticles in Metal-Organic Frameworks. *Chem. Soc. Rev.* **2013**, *42*, 1807-1824.

(16) Lu, G.; Li, S. Z.; Guo, Z.; Farha, O. K.; Hauser, B. G.; Qi, X. Y.; Wang, Y.; Wang, X.; Han, S. Y.; Liu, X. G.; DuChene, J. S.; Zhang, H.; Zhang, Q. C.; Chen, X. D.; Ma, J.; Loo, S. C. J.; Wei, W. D.; Yang, Y. H.; Hupp, J. T.; Huo, F. W. Imparting Functionality to a Metal-Organic Framework Material by Controlled Nanoparticle Encapsulation. *Nat. Chem.* **2012**, *4*, 310-316.

(17) Li, Z.; Zeng, H. C. Surface and Bulk Integrations of Single-Layered Au or Ag Nanoparticles onto Designated Crystal Planes {110} or {100} of Zif-8. *Chem. Mater.* **2013**, *25*, 1761-1768.

(18) Chen, L. Y.; Peng, Y.; Wang, H.; Gua, Z. Z.; Duana, C. Y. Synthesis of Au@Zif-8 Single- or Multi-Core-Shell Structures for Photocatalysis. *Chem. Commun.* **2014**, *50*, 8651-8654.

(19) Hu, P.; Zhuang, J.; Chou, L. Y.; Lee, H. K.; Ling, X. Y.; Chuang, Y. C.; Tsung, C. K. Surfactant-Directed Atomic to Mesoscale Alignment: Metal Nanocrystals Encased Individually in Single-Crystalline Porous Nanostructures. *J. Am. Chem. Soc.* **2014**, *136*, 10561-10564.

(20) He, L. C.; Liu, Y.; Liu, J. Z.; Xiong, Y. S.; Zheng, J. Z.; Liu, Y. L.; Tang, Z. Y. Coreshell Noble-Metal@Metal-Organic-Framework Nanoparticles with Highly Selective Sensing Property. *Angew. Chem. Int. Ed.* **2013**, *52*, 3741-3745.

(21) Pan, Y. C.; Heryadi, D.; Zhou, F.; Zhao, L.; Lestari, G.; Su, H. B.; Lai, Z. P. Tuning the Crystal Morphology and Size of Zeolitic Imidazolate Framework-8 in Aqueous Solution by Surfactants. *CrystEngcomm* **2011**, *13*, 6937-6940.

(22) Gomez-Grana, S.; Hubert, F.; Testard, F.; Guerrero-Martinez, A.; Grillo, I.; Liz-Marzan, L. M.; Spalla, O. Surfactant (Bi)Layers on Gold Nanorods. *Langmuir* **2012**, *28*, 1453-1459.

(23) Cookney, J.; Ogieglo, W.; Hrabanek, P.; Vankelecom, I.; Fila, V.; Benes, N. E. Dynamic Response of Ultrathin Highly Dense Zif-8 Nanofilms. *Chem. Commun.* **2014**, *50*, 11698-11700.

(24) Venna, S. R.; Jasinski, J. B.; Carreon, M. A. Structural Evolution of Zeolitic Imidazolate Framework-8. *J. Am. Chem. Soc.* **2010**, *132*, 18030-18033.

(25) Sentosun, K.; Sanz-Ortiz, M. N.; Batenburg, K. J.; Liz-Marzán, L. M.; Bals, S. Combination of Haadf-Stem and Adf-Stem Tomography for Core-Shell Hybrid Materials. *Part. Part. Syst. Char.* **2015**, *32*, 1063-1067.

(26) Li, S. Z.; Shi, W. X.; Lu, G.; Li, S. Z.; Loo, S. C. J.; Huo, F. W. Unconventional Nucleation and Oriented Growth of Zif-8 Crystals on Non-Polar Surface. *Adv. Mater.* **2012**, *24*, 5954-+.

(27) Nikoobakht, B.; El-Sayed, M. A. Evidence for Bilayer Assembly of Cationic Surfactants on the Surface of Gold Nanorods. *Langmuir* **2001**, *17*, 6368-6374.

(28) Peralta, D.; Chaplais, G.; Simon-Masseron, A.; Barthelet, K.; Chizallet, C.; Quoineaud, A. A.; Pirngruber, G. D. Comparison of the Behavior of Metal-Organic Frameworks and Zeolites for Hydrocarbon Separations. *J. Am. Chem. Soc.* **2012**, *134*, 8115-8126.

(29) Zhang, C.; Lively, R. P.; Zhang, K.; Johnson, J. R.; Karvan, O.; Koros, W. J. Unexpected Molecular Sieving Properties of Zeolitic Imidazolate Framework-8. *J. Phys. Chem. Lett.* **2012**, *3*, 2130-2134.

(30) Ruthven, D. M.; Loughlin, K. F. Effect of Crystallite Shape and Size Distribution on Diffusion Measurements in Molecular Sieves. *Chem. Eng. Sci.* **1971**, *26*, 577-&.

(31) Ruthven, D. M. Sorption Kinetics for Diffusion-Controlled Systems with a Strongly Concentration-Dependent Diffusivity. *Chem. Eng. Sci.* **2004**, *59*, 4531-4545.

(32) Fletcher, A. J.; Thomas, K. M.; Rosseinsky, M. J. Flexibility in Metal-Organic Framework Materials: Impact on Sorption Properties. *J. Solid. State Chem.* **2005**, *178*, 2491-2510.

(33) Ryder, M. R.; Civalleri, B.; Bennett, T. D.; Henke, S.; Rudic, S.; Cinque, G.; Fernandez-Alonso, F.; Tan, J. C. Identifying the Role of Terahertz Vibrations in Metal-Organic Frameworks: From Gate-Opening Phenomenon to Shear-Driven Structural Destabilization. *Phys. Rev. Lett.* **2014**, *113*.

(34) Nikoobakht, B.; El-Sayed, M. A. Preparation and Growth Mechanism of Gold Nanorods (Nrs) Using Seed-Mediated Growth Method. *Chem. Mater.* **2003**, *15*, 1957-1962.

(35) Zhou, N.; Polavarapu, L.; Gao, N. Y.; Pan, Y. L.; Yuan, P. Y.; Wang, Q.; Xu, Q. H. Tio2 Coated Au/Ag Nanorods with Enhanced Photocatalytic Activity under Visible Light Irradiation. *Nanoscale* **2013**, *5*, 4236-4241.

(36) Yuan, H. K.; Khoury, C. G.; Hwang, H.; Wilson, C. M.; Grant, G. A.; Vo-Dinh, T. Gold Nanostars: Surfactant-Free Synthesis, 3d Modelling, and Two-Photon Photoluminescence Imaging. *Nanotechnology* **2012**, *23*.

(37) Turkevich, J.; Stevenson, P. C.; Hillier, J. A Study of the Nucleation and Growth Processes in the Synthesis of Colloidal Gold. *Discuss. Faraday Soc.* **1951**, 55-&.

(38) W. Van Aarle , W. J. Palenstijn , J. De Beenhouwer , T. Altantzis ,S. Bals , K. J. Batenburg , J. Sijbers , Ultramicroscopy 2015 , 157 , 35